Accepted Manuscript

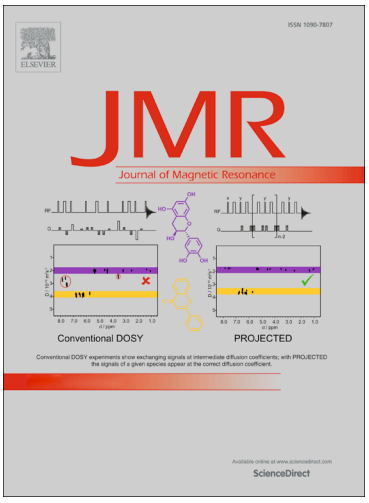

Accessing the long-time limit in diffusion NMR: the case of singlet assisted diffusive diffraction *q*-space

Giuseppe Pileio, Sylwia Ostrowska

PII: S1090-7807(17)30249-5
DOI: https://doi.org/10.1016/j.jmr.2017.10.003
Reference: YJMRE 6174

To appear in: *Journal of Magnetic Resonance*

Received Date: 7 September 2017
Revised Date: 6 October 2017
Accepted Date: 7 October 2017

Please cite this article as: G. Pileio, S. Ostrowska, Accessing the long-time limit in diffusion NMR: the case of singlet assisted diffusive diffraction *q*-space, *Journal of Magnetic Resonance* (2017), doi: https://doi.org/10.1016/j.jmr.2017.10.003

Accessing the long-time limit in diffusion NMR: the case of singlet assisted diffusive diffraction *q*-space

Giuseppe Pileio* and Sylwia Ostrowska

School of Chemistry, University of Southampton, SO17 1BJ, Southampton, U.K

Abstract

The latest developments in the field of long-lived spin states are merged with pulsed-field gradient techniques to extend the diffusion time beyond what is currently achievable in standard *q*-space diffusive-diffraction studies. The method uses nearly-equivalent spin-1/2 pairs that let diffusion times of the order of many minutes to be measured allowing access to the long-time limit in cavities of macroscopic size (millimeters). A pulse sequence suitable to exploit this regime has been developed and validated with the use of numerical simulations and experiments.

Keywords

Long-lived states; *q*-space; Diffusion; Diffusive-diffraction; Magnetic Resonance;

Highlights

- A pulse sequence based on Magnetisation-to-Singlet transfers and pulsed field gradients is developed and validated using experiments and numerical simulations
- Singlet-enhanced *q*-space diffraction allows measurement in the long-time limit
- *q*-space diffraction capabilities in measuring compartment sizes have been extended from hundreds of microns to a few millimeters

*corresponding author: g.pileio@soton.ac.uk

Graphical abstract

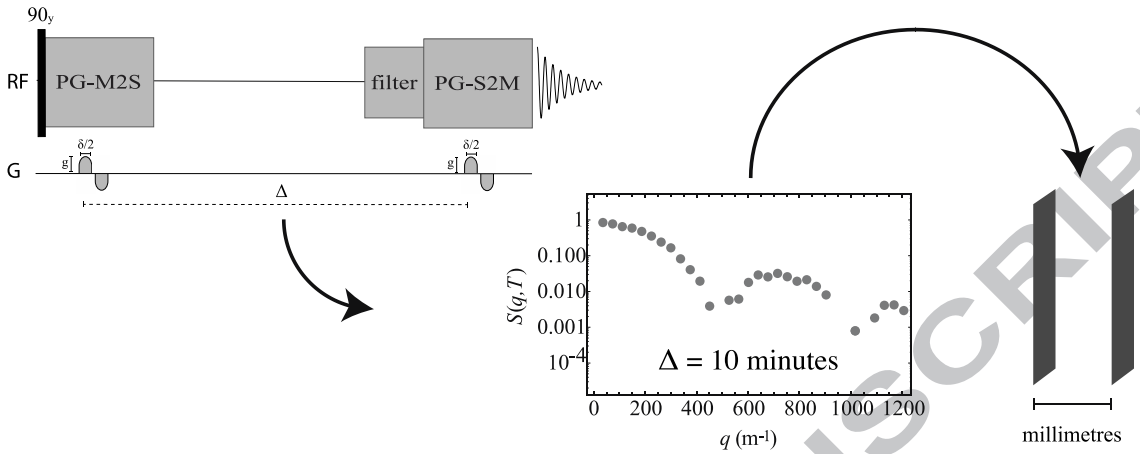

1. Introduction

Molecular translational motions such as flow, free and restricted diffusion, convection *etc.* can be studied with nuclear magnetic resonance techniques.[1-3] Generally speaking, all methods rely on preparing some form of spin order (at a given position and time), then following its fate as the molecules undergo the translational motion of interest. Clearly, spin order must survive the duration for which the motion is to be studied and, consequently, all these techniques are limited by the characteristic decay rate of the spin order prepared. The two main pulse sequences in this area are the pulsed gradient spin echo[4] (PGSE) and the pulsed gradient stimulated echo[5] (PGSTE). Both these sequences use pulsed magnetic field gradients to encode and, later on, decode the molecular position. The PGSE method creates transverse spin order whose characteristic decay time is conventionally indicated as T_2 whereas the PGSTE method creates longitudinal spin order whose characteristic decay time is indicated as T_1. For small molecules in low-viscosity solvents and at high magnetic field strength $T_1 \sim T_2$ and the PGSE experiment is preferred because it can deliver twice as much signal as the PGSTE. Outside of this condition typically $T_2 < T_1$ and therefore the PGSTE is preferred.

In the most common practice, the intensity of the signal acquired at the end of these sequences is plotted as a function of the gradient strength or measurement time. The decaying signal can be fit to theoretical or empirical models (see Theory section below) to yield information on the diffusion coefficient, the pore size, porosity and many other structural parameters of the material in which the molecules are imbibed.[6]

When dealing with molecules confined in a restricted space, the measured diffusion coefficient appears smaller than when molecules diffuse in an unrestricted environment.[3] In the event of relatively mono-disperse compartment sizes, strong spatial coherence between the diffusing spins causes minima in the intensity of the signal at selected and equally spaced values of the gradient strength. These can be correlated with the characteristic size of the restricting geometry. Such experiments have been termed as *diffusive diffraction* in analogy with X-ray diffraction. In the NMR field, the diffusive diffraction technique is also known as *q-space diffraction* for the reasons that will be clear below. Given the ability of *q*-space diffraction to obtain information on geometry, the technique has been widely used to characterize sizes and shapes in porous media relevant to various disciplines ranging from material sciences[3, 7-16] to medicine[17-20], including a form of NMR-based cytology[21-22]. However, the largest measurable size of pores and compartments is limited to about 50-100

μm due to the "limited" time that longitudinal order survives while molecules diffuse in a medium.

More recently, long-lived spin order was used in NMR diffusion experiments[23-27] and, more relevant to this paper, in diffusive diffraction *q*-space measurements[28-29]. Thanks to the fact that long-lived spin order has a characteristic decay time, T_S, which is typically one order of magnitude bigger than T_1, these singlet-enhanced *q*-space experiments have extended the scope of *q*-space spectroscopy to cavity sizes of up to ~400 μm.[29] However, those singlet-enhanced diffusion methods are no longer up-to-date with the developments in the field of long-lived spin order and can therefore be improved. The methodology used in those pioneering papers[28-29] requires the use of a spin-locking radiofrequency field turned on for the length of the diffusion period. This constitutes a fundamental limit in the sense that, if the required radiofrequency field is "too strong" and/or the diffusion time "too long" one can incur sample heating (with connected convection issues) and, in the worst case, damage to the probe. Because of this, the diffusion time must be kept within specific hardware limits. Furthermore, singlet-bearing molecules suitable for these spin-locking methods, have singlet order lifetimes which are longer than T_1 but, typically, not very long in absolute terms. For these reasons, the benefits of using spin-locking singlet diffusing methods instead of more conventional techniques (not based on singlet order) is not spectacular.

In this paper, we consolidate the latest developments in the field of long-lived spin order and merge them with diffusion NMR standard techniques to obtain a method that is able to exploit diffusion times of the order of tens of minutes, and possibly much longer depending on the molecular spy. We demonstrate the use of this technique in the context of *q*-space diffraction to measure compartment sizes of the order of a few millimeters.

2. Theory

When molecules diffuse in a medium, the total probability density that a particle is found at position *r* at time *t* is given by[3]:

$$P(r,t) = \int \rho(r) P(r_0|r,t) dr \qquad (1)$$

with $\rho(r)$ being the particle density and $P(r_0|r,t)$ the conditional probability density that a particle is found at position *r*, at time *t* after having been at position r_0 at time $t_0 = 0$.

The conditional probability density above fulfills Fick's second law:

$$\frac{dP(r_0|r,t)}{dt} = D\nabla^2 P(r_0|r,t) \quad (2)$$

with *D* indicating the diffusion coefficient. Eq. 2 can be solved analytically only in a few regimes. In the case of freely-diffusing particles in one dimension, the solution can be derived using the method of the Fourier transform to obtain:

$$P(z_0|z,t) = \frac{1}{\sqrt{4\pi Dt}} e^{-\frac{(z-z_0)^2}{4Dt}} \quad (3)$$

If diffusion happens in a restricted geometry, then the solution of Eq. 2 becomes more complicated. However, for a few simple geometries an analytical solution is available. One such example, relevant to this work, is the case of molecules diffusing between perfectly reflecting walls separated by a distance *l*. In this case (still in one dimension for the sake of simplicity), the conditional probability of Eq. 2 assumes the form[30]:

$$P(z_0|z,t) = \frac{1}{l} + \frac{2}{l}\sum_{n=1}^{\infty} cos\left(\frac{n\pi}{l} z_0\right) cos\left(\frac{n\pi}{l} z\right) e^{-\frac{n^2\pi^2 Dt}{l^2}} \quad (4)$$

with analogous equations available when diffusion happens within spherical and cylindrical compartments.[3, 31]

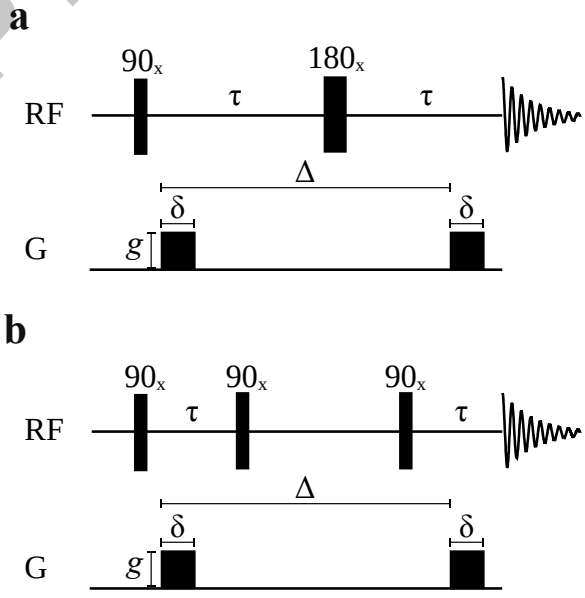

Fig. 1: A sketch of a) pulsed-gradient spin echo (PGSE) and b) pulsed-gradient stimulated echo (PGSTE) pulse sequences. RF refers to the radiofrequency channel we 90 degrees and 180 degree pulse are applied along the x-axis (90x and 180x, respectively), G to the gradient channel, g is the gradient pulse strength, δ is the gradient duration, Δ is the diffusion delay and τ is the echo delay.

The most basic NMR diffusion pulse sequence (PGSE) is shown in Fig. 1a. If one assumes that the duration of the gradient is negligible (i.e. $\delta \ll \Delta$, *narrow-pulse approximation*) then the effect of the field gradient is to impart a phase shift $\gamma\delta g z_0$ to spins located at position z_0. After the application of both gradients, and neglecting spin relaxation, the intensity of the signal at the echo point is given by:

$$S(g,t) = \int \rho(z_0) \int P(z_0|z,t) e^{i2\pi q(z-z_0)} dz dz_0 \tag{5}$$

Attenuation of the signal in Eq. 5 is the result of the net phase shift that a spin accumulates when it reaches position *z* at the time of the second field gradient pulse (at $t = \Delta$) having been at position z_0 at the time of the first field gradient pulse ($t = 0$). The central quantity:

$$q = \frac{\gamma\delta g}{2\pi} \tag{6}$$

has the dimension of m^{-1} and gives the name to the *q*-space technique.

Assuming that molecules are equally distributed in space at time $t = 0$, the NMR signal at the echo point of a PGSE experiment (for freely diffusing molecules in one dimension) is found by inserting Eq. 3 into Eq. 5 to obtain:

$$S_f(q,\Delta) = \int \frac{1}{\sqrt{4\pi D\Delta}} e^{-\frac{(z-z_0)^2}{4D\Delta}} e^{i2\pi q(z-z_0)} dz dz_0 = e^{-(2\pi q)^2 D\Delta} \tag{7}$$

A plot of $S_f(q,\Delta)$ (*f* indicates free diffusion) versus *q* and for $\Delta = 10$ s and $D = 2.0 \times 10^{-9}$ $m^2 s^{-1}$ is shown in Fig. 2 (grey line). In the case of diffusion between parallel planes, where the propagator is given by Eq. 4, the signal at the echo point of a PGSE experiment has the analytical form:

$$S_{\parallel}(q,\Delta) = \frac{sin(l\pi q)}{(l\pi q)^2} + (4lq)^2 \sum_{n=1}^{\infty} \left[\frac{1-(-1)^n cos(2\pi lq)}{\pi^2(n^2-4l^2q^2)^2}\right] e^{-\frac{n^2\pi^2 D\Delta}{l^2}} \tag{8}$$

Note the features (*diffraction minima*) that appear at $q \times l = k$ (with the integer $k = 1, 2, \ldots$). The position of these minima gives direct information about the geometrical parameters of the space the molecules are diffusing within (in this simple case the wall distance *l*). A plot of

$S_{\parallel}(q,\Delta)$ ($\parallel$ indicates diffusion restricted by parallel planes) versus q and for Δ = 10 s, D = 2.0 × 10^{-9} m^2s^{-1} and l = 100 μm is also shown in Fig. 2 (black line).

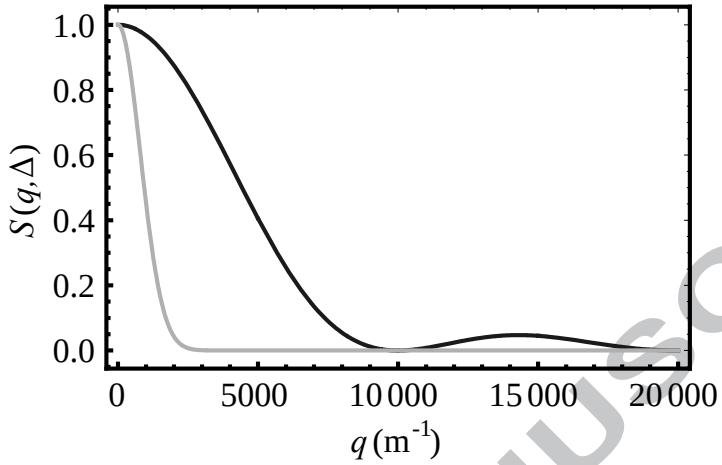

Fig. 2: A plot of the analytical form of S(q,Δ) in Eq. 7 (grey line) and Eq. 8 (black line) versus q and for D = 2.0 × 10⁻⁹ m² s⁻¹, Δ = 10 s and l = 100 μm (plot done using Wolfram Mathematica 11.)

Two limiting behaviours are worth noticing: *i*) the short time-limit (*short*), defined by the condition $\Delta \ll l^2/(2D)$, for which Eq. 8 reduces to:

$$S_{\parallel}^{short}(q,\Delta) = e^{-(2\pi q)^2 D\Delta} \tag{9}$$

Note that this is the same as the expression obtained in the free diffusion case (see Eq. 7); and *ii*) the long-time limit (*long*), defined by the condition $\Delta \gg l^2/(2D)$, for which Eq. 8 reduces to:

$$S_{\parallel}^{long}(q,\Delta) = S_{\parallel}(q) = \frac{sin(l\pi q)}{(l\pi q)^2} \tag{10}$$

In this regime the NMR signal becomes independent of both the diffusion time Δ and the diffusion coefficient D. Similar equations, derived for the more general case in which the walls are not perfectly reflecting (i.e. including a term to account for spin relaxation occurring at the walls), are available in literature[31-33].

Spin relaxation during the experiment (transverse for PGSE and longitudinal for PGSTE) also contributes to signal decay and poses an upper limit to Δ, which in turn limits the largest value of l measurable via a PGSE or PGSTE technique. Consequently, the long-

time diffusion limit cannot be reached in geometries whose characteristic sizes are above a threshold that is defined by the absolute value of T_1. This limit is of the order of 100 μm.

3. The PGM2S2M pulse sequence

In order to access the long-time limit for geometries whose characteristic dimensions exceed this limit we have developed, implemented and tested a pulsed-gradient magnetisation-to-singlet-to-magnetisation pulse sequences (PGM2S2M) that uses long-lived singlet spin order to store molecules' positional information for a time exceeding T_1 (typically an order of magnitude or more). The PGM2S2M pulse sequence is sketched in Fig. 3.

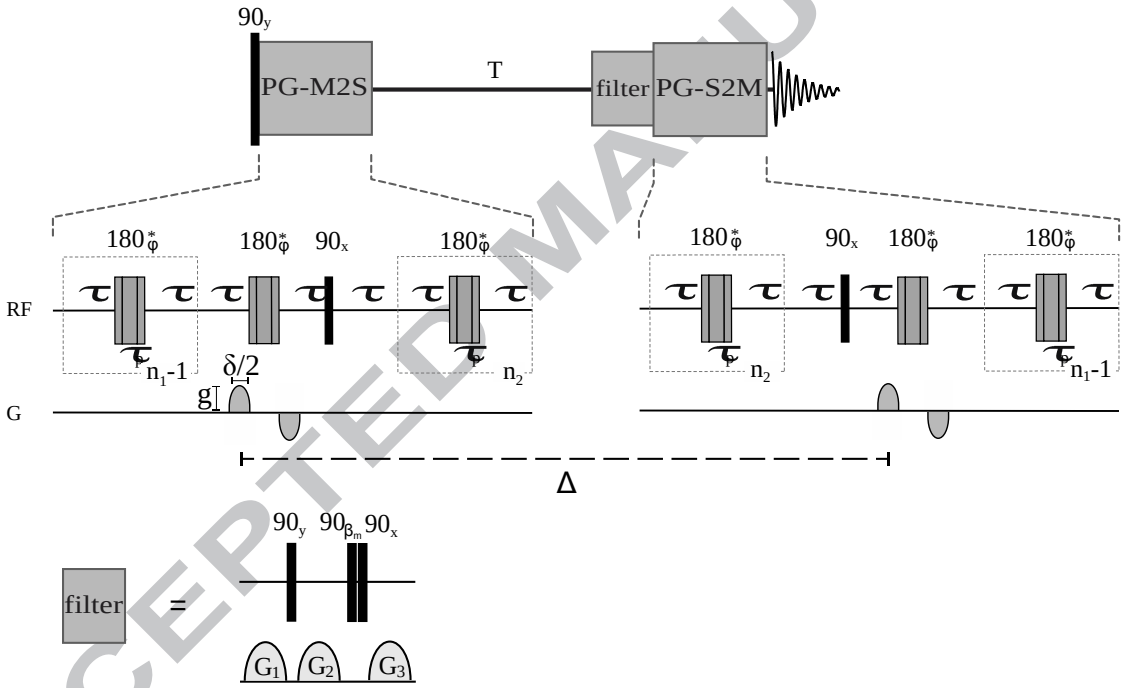

Fig. 3: A sketch of the PGM2S2M pulse sequence to perform q-space diffraction NMR experiment in the long-time limit. Asterisks indicate a composite 180° pulse built as $90_x180_y90_x$. The phase φ is cycled as [x,x,-x,-x,-x,x,x,-x,-x,-x,x,x,-x,-x,x] within the train of 180° pulses. The total echo time is given as $\tau_e = \tau_p + 2\tau = 1/(2\sqrt{J^2 + (\Delta\nu)^2})$ with τ_p the duration of the composite 180° pulse. $n_1 = \pi J/(2\Delta\nu)$ and $n_2 = n_1/2$. All gradients have sinusoidal shape and $\beta_m = arctan(\sqrt{2})$.

An initial 90 degrees pulse generates transverse magnetisation, $(I_{1x} + I_{2x})$. The successive PG-M2S is a simple modification of the conventional M2S sequence[34-35] where the introduction of a bipolar gradient placed around the composite 180° pulse is used to encode the spatial position of nuclear spins. Although the bipolar gradient pulse could be placed at any point during the n_1-echo-train (but not later), it was placed during the last echo in order to minimize the smallest diffusion time achievable with the pulse sequence. At the end of the

PG-M2S block, neglecting relaxation and hardware imperfections, 2/3 of the initial magnetisation is converted into long-lived singlet order, $(I_1^+ I_2^- + I_1^- I_2^+)$. Successively, a delay *T* is inserted and adjusted so as to obtain the desired value of Δ by taking into account the duration of all other pulse blocks placed between the first and the last bipolar gradient. At the end of the delay *T*, a singlet-order filter[36] is inserted. The filter allows only singlet order to pass to the following part of the sequence where a PG-S2M (obtained by time-reversing the PG-M2S) converts singlet order back into transverse magnetisation, $(I_{1x} + I_{2x})$, while simultaneously decoding positional information via a second bipolar field gradient pulse. An in-depth explanation of the spin order transformations carried out by the M2S and S2M block is available in literature.[37]

In a typical experiment the value of τ, n_1, n_2 are experimentally adjusted around their theoretical values ($\tau_e = \tau_p + 2\tau = 1/(2\sqrt{J^2 + (\Delta\nu)^2})$ and $n_1 = \pi J/(2\Delta\nu)$, with τ_p the duration of the composite 180° pulse), so as to maximize the magnetisation-to-singlet conversion efficiency; the values of δ and Δ are also fixed while the gradient strength *g* is varied in a number of linearly-spaced steps. The signal acquired varies with *q* as described by Eqs. 7 and 8 in the case of unrestricted and restricted (parallel planes) diffusion, respectively.

4. Results and Discussion

4.1 Numerical Simulations

To validate the proposed methodology, numerical spin-dynamics simulations of the pulse sequences in Fig. 1 and 3 have been run using a custom-made code (available upon request) programmed in Wolfram Mathematica 11. Molecular diffusion was handled using the following strategy:

a. *initial configuration:* a number of *N* positions have been randomly distributed along the z-axis in the interval [-*l*/2, *l*/2], with *l* indicating the linear dimension in meters. This results in an array of *N* initial positions labeled $\{z_i^1, z_i^2, \dots, z_i^N\}$.

b. *final configuration:* for each k^{th} position, a final position is calculated by extracting a random number from a normal distribution with mean z_i^k and standard deviation $\sigma = \sqrt{2Dt}$. This results in an array of *N* final positions labeled $\{z_f^1, z_f^2, \dots, z_f^N\}$.

c. The Hamiltonian describing the effect of the pulsed field gradient is implemented as $H_G = \gamma g\, z_t^k\, I_z$ where z_t^k refers to one of the *N* positions along the z-axis at the time of the gradient, i.e. the set $z_t^k = \{z_i^1, z_i^2, \dots, z_i^N\}$ for the first bipolar gradient and

$z_t^k = \{z_f^1, z_f^2, \ldots, z_f^N\}$ for the second one. Diffusion during the gradient is neglected although spin evolution is fully accounted for.

d. The amplitude of the transformation from the initial longitudinal spin order I_z (at the start of the pulse sequence) into the final transverse spin order I_x (at the start of acquisition, see Fig. 3) is calculated using custom-made routines written in Mathematica (Wolfram Research Inc., Champaign, Illinois) and that make use of the SpinDynamica package[38]. In order to account for the gradient and the diffusion effects, *N*n* transformation amplitudes calculations are made, one for each $[z_i^k, z_f^k]$ pair and for each of the *n* steps in the arrayed value of *g*.

e. Finally, an ensemble average over the *N* positions is taken by summing up all calculated amplitudes for each of the *n* values of *g*. All simulations neglect spin relaxation phenomena.

This simulation strategy was firstly validated by simulating two well-known examples, PGSE and PGSTE, in the case of unrestricted diffusion (Fig. 1a and b). These simulations assume *N* = 5000 molecular positions distributed along the z-direction and within parallel walls separated by *l* = 0.5 mm. The diffusion coefficient was assumed $D = 1.0 \times 10^{-9}$ m^2 s^{-1}, δ = 0.5 ms, τ = 5 ms and Δ = 1 s, to mimic unrestricted diffusion conditions. The value of *g* was arrayed in 16 equally spaced steps between 0 and 1.5 T m^{-1}. The simulated system is made by two spin-1/2 nuclei with a difference in chemical shift frequencies $\Delta\nu = 1.18\ Hz$ and a scalar coupling $J = 12\ Hz$, chosen to mimic the experimental case discussed below (see Scheme 1).

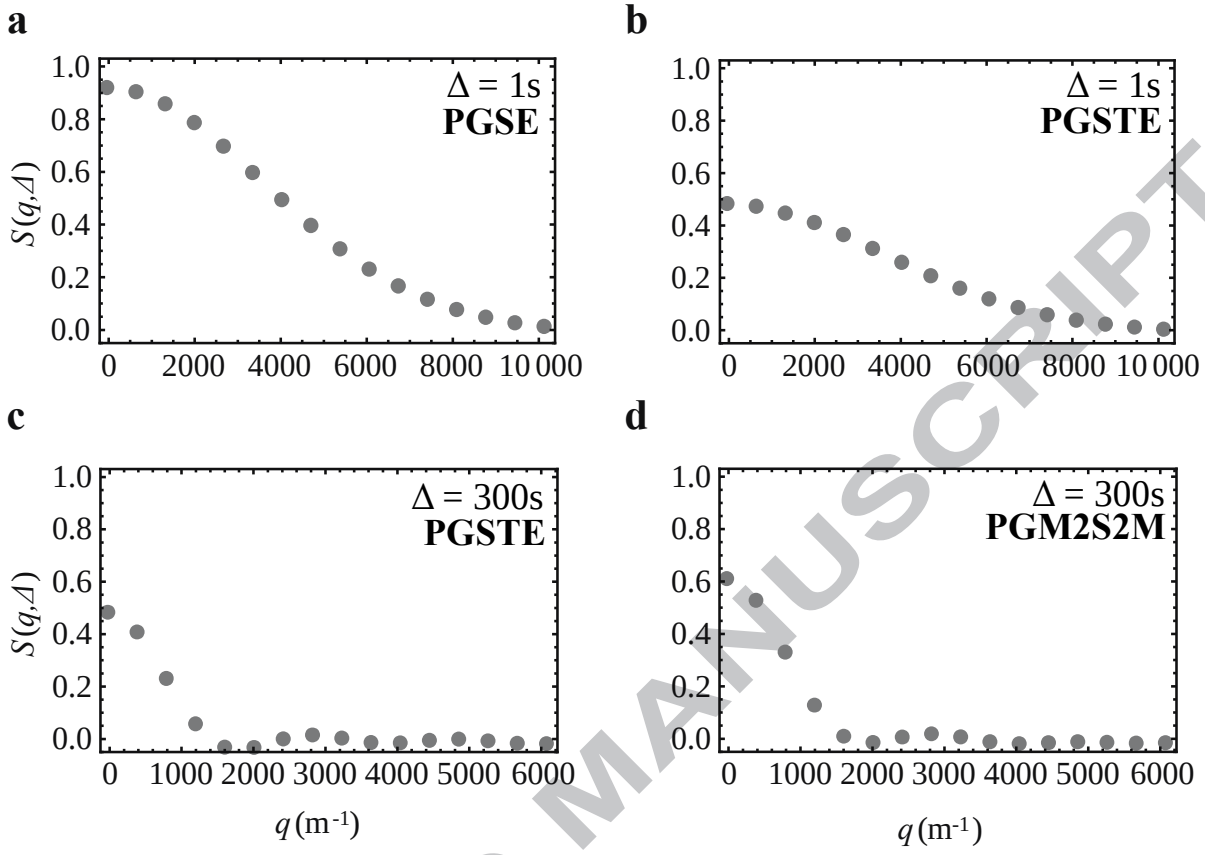

Fig. 4: Numerical simulations of the pulse sequences in Fig. 1 and 3 done using custom made routines that use the SpinDynamica package[38]. All simulations follow the strategy described in Sec. 3 with N = 5000, l = 0.5 mm, D = 1.0 × 10^{-9} m^2 s^{-1}, δ = 0.5 ms, τ = 5 ms and Δ as indicated. The value of g was arrayed in 16 equally spaced steps between 0 and 1.5 T m^{-1}. The simulated system is made by two spin-1/2 with a difference in chemical shift frequencies Δν = 1.18 Hz and a scalar coupling J = 12 Hz. a) simulation of a PGSE experiment in the case of unrestricted diffusion; b) simulation of a PGSTE experiment in the same case of unrestricted diffusion; c) simulation of a PGSTE experiment in the case of diffusion between parallel walls separated by l = 0.5 mm and for Δ = 300 s; d) simulation of a PGM2S2M experiment in the case of diffusion between parallel walls identical to c).

The simulated curves have the expected shape and were fitted to retrieve the correct diffusion coefficient. The reduction in intensity by half when using PGSTE instead of PGSE (compare Fig. 1a and b) is well-known and due to the fact that only the y-component of the transverse magnetisation generated after the very first 90x pulse can be converted into longitudinal magnetisation by a second 90x pulse.[3] The simulation results in Fig. 1c and d compare PGSTE and PGM2S2M in the case of restricted diffusion. These simulations use the same parameters as Fig. 1a and b but with Δ set to 300 s to allow molecules to reach, and be reflected by, the walls (relaxation at the walls was neglected for the sake of simplicity). The simulated curves display diffraction minima at q = 2000 and 4000 m^{-1} consistent with the theory. The intensity of the first point at q = 0 m^{-1} (i.e. g = 0 T m^{-1}) in Fig. 1d is very close to 2/3 (slightly lower due to rounding the values of n_1 to the nearest even integer), which is the maximum theoretical amplitude transfer for the transformation of magnetization-to-singlet-to-

magnetisation achievable with unitary transformations. Experimentally, the observed conversion amplitude for the transformation between longitudinal and singlet order is often lower than theoretical predictions.[37] This has been attributed to relaxation phenomena happening during the pulse sequence and hardware imperfections, which are not included in these simulations. Despite these relaxation losses and imperfections, the PGM2S2M compares well to the PGSTE and PGSE with regard to signal intensity. The theoretical amplitude of the first point in a PGSTE experiment is 0.5 (also affected by relaxation and hardware imperfections) while the PGSE experiment is affected by magnetisation evolution under scalar coupling, and other coherent phenomena during Δ. Therefore, the intensity of the first point depends on the value of Δ. In the simulated case, because in the presence of a nearly-equivalent spin pair (i.e. $\Delta\nu \ll J$), the transverse magnetisation in a PGSE experiment oscillates at the small frequency difference between the two inner transitions of the AB pattern i.e. at $\nu_{in} = \left(\sqrt{\Delta\nu^2 + J^2} - J\right)/2 \sim 30$ mHz which can lead to significant losses of intensity for long Δ values. Finally, and most importantly, the PGM2S2M has the great advantage over the other two methods of being able to access significantly longer values of Δ. This is evident in the experiments discussed below.

4.2 *q*-space NMR Experiments

4.2.1 Samples and methods

To test the capabilities of the proposed method, singlet-enhanced *q*-space diffraction NMR experiments were used to measure the shortest dimension (defined as the depth below) of three different rectangular capillary tubes. The capillaries, sized **A**) 50×8×0.4 mm, **B**) 50×8×0.8 mm and **C**) 48×4×2 mm (L×W×D, internal dimensions, 10% precision), were purchased from Wale Apparatus (Hellertown, US) in the case of **A** and **B** and from CM Scientific (Silsden, UK) in the case of **C**. Each of these three capillaries has been fused to the J-Young valve of a 10 mm OD gas-tight LPV NMR tube for support and to allow degassing. Each of these three resulting (capillary) tubes has been filled with a solution 0.9 M of 1-(ethyl-d5),4-(propyl-d7)(*Z*)-but-2-enedioate (Scheme 1, a custom-made singlet-bearing molecule that possesses a long singlet-order lifetime[39-40] and that is easily available in our laboratory) in deuterated methanol for the tube carrying capillary **A** and in deuterated acetone for those carrying capillaries **B** and **C**. The solutions were degassed through a three step pump-thaw cycle in order to remove dissolved oxygen.

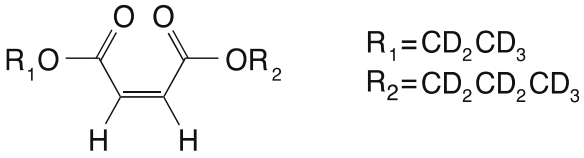

Scheme 1: Molecular scheme of 1-(ethyl-d5) 4-(propyl-d7)(Z)-but-2-enedioate used in all experiments discussed in this paper

All experiments were run on a Bruker 11.7 T Avance III NMR instrument equipped with a 10 mm $^{1}H/^{13}C$ resonator and a gradient system able to deliver pulsed field gradients of up to 1.5 T m^{-1}. The capillaries were placed in the NMR probe and their alignment adjusted until their width (see specifications above) was perpendicular to the y-axis gradient as determined by the width of the y-profile obtained by running a 1D imaging experiment with field gradient pulses on that axis. All experiments have been run at room temperature (21 ^{o}C) and without using the probe's temperature controller to achieve a more sample temperature and minimize convection flow.

4.2.2 Experiments

Sample **A** was used to optimize the basic parameters in the PGM2S2M sequence; these were found to be: τ = 20.8 ms, n_1 = 16 and n_2 = 8. A standard saturation recovery experiment measured a T_1 decay constant of 15.5 ± 0.1 s. The singlet order decay constant was measured using the M2S2M method[37] and was found to be T_S = 250 ± 10 s. The unrestricted diffusion coefficient was measured using PGSTE (with bipolar gradients, Δ = 200 ms and δ = 3 ms) and was found to be $D_0 = 7.7 \times 10^{-10}$ m^2 s^{-1}.

Sample **A** was then used to test the capabilities of the PGM2S2M pulse sequence (Fig. 3) at four diffusion times: Δ = 15 s, 30 s, 3 min and 5 min (Fig. 5a-d). In these experiments, the value of δ was kept fixed at 2 ms (note that in all cases $\delta \ll \Delta$, *narrow-pulse approximation*) while the strength of the gradient g was varied between 1.5 mT m^{-1} and 105 mT m^{-1} in 21 linearly spaced steps. The gray points in Fig. 5 are the signal area plotted against q whereas the solid curve is an overlay of the plot of Eq. 8 for the exact case of l = 0.4 mm (characteristic dimension of sample **A**) and $D_0 = 7.7 \times 10^{-10}$ m^2 s^{-1}. For this geometry, $l^2/(2D_0) \cong 100$ s and the long-time limit is reached for $\Delta \gg 100$ s. Results in Fig. 5 show that PGSE/PGSTE experiments, limited by T_1 (in this case ~15 s), would fail to measure compartments of such sizes and above (see Fig. 5a and b). Conversely, singlet-enhanced q-space experiments, obtained with the use of the PGM2S2M pulse sequence, can successfully detect the diffraction minima occurring at $q \times l = integer$ (only the first 2 shown, see Fig. 5c

and d) as expected for the case of molecular diffusion restricted between parallel walls separated by *l*.

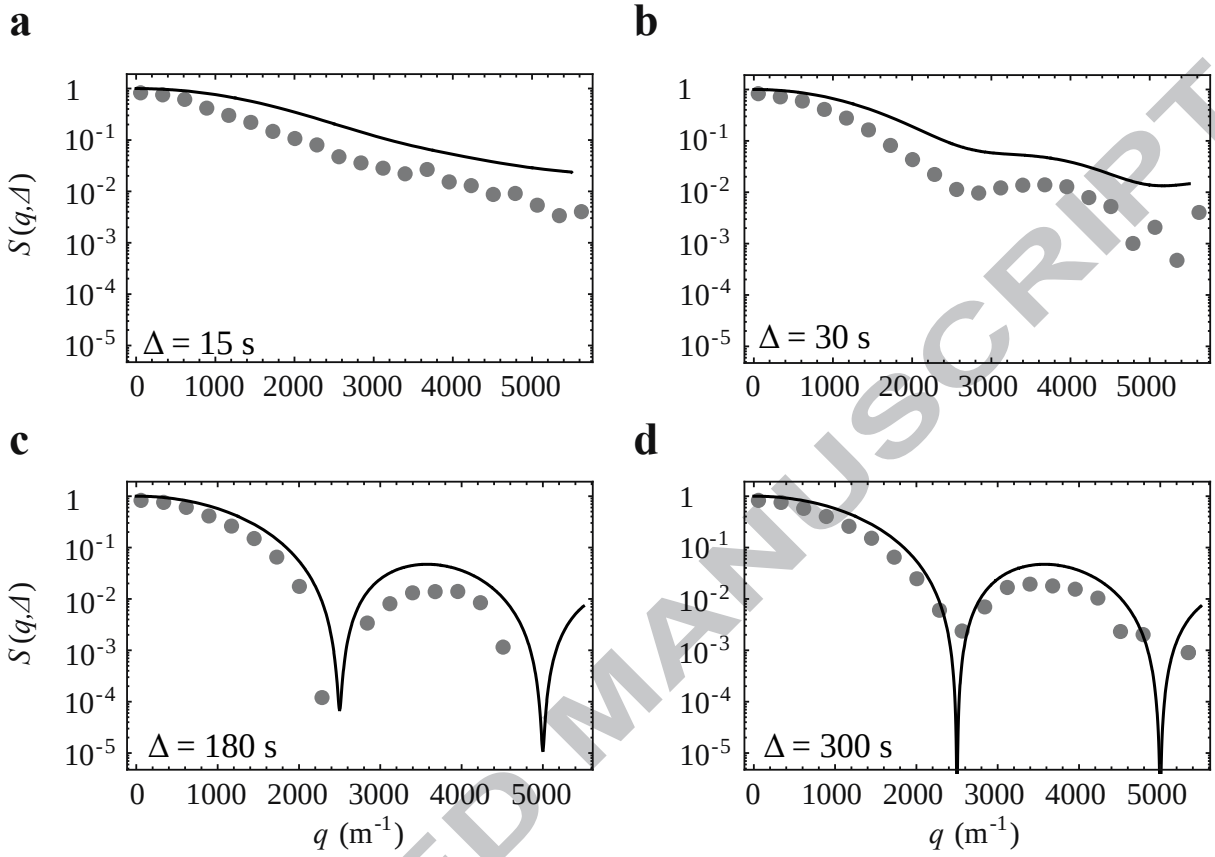

*Fig. 5: q-space logarithm plots of signal area versus q for capillary **A** (l = 0.4 ± 0.04 mm) at four different values of the diffusion time Δ (as indicated). Experimental points are in gray; solid lines are a plot of Eq. 8 for l = 0.4 mm and D_0 =7.7 × 10^{-10} m^2 s^{-1}.*

In order to probe the new limits of the technique, now limited by T_S rather than T_1, we ran the PGM2S2M pulse sequence to measure the intensity of the NMR signal as a function of *q* for the rectangular capillaries **B** and **C** whose characteristic dimensions are l = 0.8 ± 0.08 and l = 2.0 ± 0.2 mm (see Fig. 6). The value of Δ was 7 min for **B** and 10 min for **C**. The diffusion coefficient of the compound in Scheme 1 dissolved in acetone-d_6 was found to be D_0 = 1.6 × 10^{-9} m^2 s^{-1}. The value of δ was kept at 2 ms while the strength of the bipolar gradient, *g*, was varied between 1.5 mT m^{-1} and 60 mT m^{-1} in 40 linearly spaced steps for **B** and between 0.75 mT m^{-1} and 22.5 mT m^{-1} in 32 linearly spaced steps for **C**. The results of these experiments are reported in Fig. 6 (gray points). In the same figure the experimental data are fitted to Eq. 10 to yield l = 0.756 ± 0.002 and l = 2.06 ± 0.02 for **B** and **C**, respectively (Fig. 6a and b). These values are well within the capillaries' tolerances given by the manufacturer indicating the ability of this singlet-enhanced *q*-space diffraction technique to measure compartment sizes in the region of a few millimeters; an order of magnitude larger than what is currently accessible by PGSE and PGSTE techniques. These sizes are also

significantly larger than those reached with previously proposed singlet-enhanced *q*-space methods.[28-29] These studies were limited due to their use of the long-lived order available in systems of two spin-1/2 when magnetic symmetry is imposed by the use of a radiofrequency field.[41]

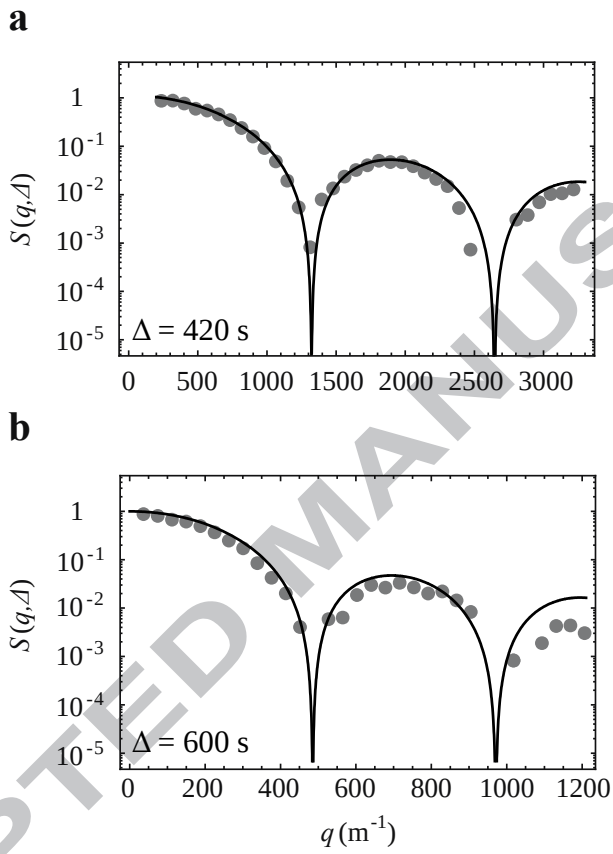

Fig. 6: q-space logarithmic plots of signal area versus q for a) capillary B with l = 0.8 ± 0.08 mm and b) capillary C with l = 2.0 ± 0.2 mm. Experimental points are in gray; solid lines are the best fit to Eq. 10.

This methodology is fundamentally limited by the fact that the singlet bearing molecules suited for this method, display lifetimes longer than T_1 but with an absolute magnitude that is often not very large (typically of the order or 10-100 s). As explained above, even in the case of such molecules having significantly longer singlet order lifetimes, hardware limitations will prevent access to significantly longer diffusion times. Conversely, the methodology proposed in this paper can be run at any magnetic field strength and does not require continuous radiofrequency irradiation. Furthermore, molecules suited for the method proposed in this work, often display singlet order lifetimes that are many minutes[42-43] up to hours[44] in length. This is the key to accessing larger compartment sizes.

6. Conclusions

We have introduced a method which extends the long-time diffusion limit in *q*-space diffusion diffraction experiments by an order of magnitude to measure compartment sizes of up to 2 mm. This is well beyond the limits of current *q*-space experiments based on PGSE or PGSTE pulse sequences, and previous *q*-space measurements that have used singlet-order. The effect of wall relaxation has been deliberately omitted in this work and is currently under study. Singlet order is immune to internal gradients and, providing one can access singlet order in the presence of such gradients, this technique may be advantageous over traditional methods when working with real systems. Here, susceptibility inhomogeneities do cause large internal gradients that typically compromise, or at least complicate, NMR diffusion measurements. We are working on verifying this hypothesis and, in the case of large susceptibility differences, developing an apparatus to perform these experiments in low magnetic field, where internal gradients are largely minimized.

Acknowledgments

The authors thank Linda J. Brown for experimental help and EPSRC for funding (grant no.: EP/N033558/1).

References

1. Callaghan, P. T., *Principles of Nuclear Magnetic Resonance Microscopy*. Clarendon Press: Oxford, 1993.
2. Price, W. S., *NMR studies of translational motion*. Cambridge University Press: Cambridge, 2009.
3. Callaghan, P. T., *Translational dynamics & magnetic resonance*. Oxford University Press: Oxford, 2011.
4. Stejskal, E. O.; Tanner, J. E., Spin diffusion measurements: spin echoes in the presence of a time-dependent field gradient. *The Journal of Chemical Physics* **1965,** *42* (1), 288-292.
5. Tanner, J. E.; Y., C. H.; M., P. E., Use of the stimulated echo in NMR diffusion studies. *The Journal of Chemical Physics* **1970,** *52* (5), 2523-2526.
6. Kärger, J.; Valiullin, R., Diffusion in porous media. In *eMagRes*, John Wiley & Sons, Ltd: 2007.
7. Callaghan, P. T.; Coy, A.; MacGowan, D.; Packer, K. J.; Zelaya, F. O., Diffraction-like effects in NMR diffusion studies of fluids in porous solids. *Nature* **1991,** *351* (6326), 467-469.
8. Callaghan, P. T.; MacGowan, D.; Packer, K. J.; Zelaya, F. O., High-resolution q-space imaging in porous structures. *Journal of Magnetic Resonance (1969)* **1990,** *90* (1), 177-182.
9. D'Agostino, C.; Gladden, L. F.; Mantle, M. D.; Abbott, A. P.; Ahmed, E. I.; Al-Murshedi, A. Y.; Harris, R. C., Molecular and ionic diffusion in aqueous - deep eutectic solvent mixtures: probing inter-molecular interactions using PFG NMR. *Phys Chem Chem Phys* **2015,** *17* (23), 15297-304.
10. Blythe, T. W.; Sederman, A. J.; Mitchell, J.; Stitt, E. H.; York, A. P.; Gladden, L. F., Characterising the rheology of non-Newtonian fluids using PFG-NMR and cumulant analysis. *J Magn Reson* **2015,** *255*, 122-31.
11. Weber, D.; Sederman, A. J.; Mantle, M. D.; Mitchell, J.; Gladden, L. F., Surface diffusion in porous catalysts. *Phys Chem Chem Phys* **2010,** *12* (11), 2619-24.

12. Sankey, M. H.; Holland, D. J.; Sederman, A. J.; Gladden, L. F., Magnetic resonance velocity imaging of liquid and gas two-phase flow in packed beds. *J Magn Reson* **2009,** *196* (2), 142-8.
13. Hollingsworth, K. G.; Sederman, A. J.; Buckley, C.; Gladden, L. F.; Johns, M. L., Fast emulsion droplet sizing using NMR self-diffusion measurements. *J Colloid Interface Sci* **2004,** *274* (1), 244-50.
14. Tomer, G.; Mantle, M. D.; Gladden, L. F.; Newton, J. M., Measuring water distribution in extrudates using magnetic resonance imaging (MRI). *Int J Pharm* **1999,** *189* (1), 19-28.
15. Harding, S. G.; Gladden, L. F., Diffusion of liquids into semicrystalline polyethylene. *Magn Reson Imaging* **1998,** *16* (5-6), 647-9.
16. Harding, S. G.; Johns, M. L.; Pugh, S. R.; Fryer, P. J.; Gladden, L. F., Magnetic resonance imaging studies of diffusion in polymers. *Food Addit Contam* **1997,** *14* (6-7), 583-9.
17. Kuchel, P. W.; Coy, A.; Stilbs, P., NMR "diffusion-diffraction" of water revealing alignment of erythrocytes in a magnetic field and their dimensions and membrane transport characteristics. *Magnetic Resonance in Medicine* **1997,** *37* (5), 637-643.
18. Waudby, C. A.; Mantle, M. D.; Cabrita, L. D.; Gladden, L. F.; Dobson, C. M.; Christodoulou, J., Rapid distinction of intracellular and extracellular proteins using NMR diffusion measurements. *J Am Chem Soc* **2012,** *134* (28), 11312-5.
19. Avram, L.; Assaf, Y.; Cohen, Y., The effect of rotational angle and experimental parameters on the diffraction patterns and micro-structural information obtained from q-space diffusion NMR: implication for diffusion in white matter fibers. *J Magn Reson* **2004,** *169* (1), 30-8.
20. King, M. D.; Houseman, J.; Roussel, S. A.; van Bruggen, N.; Williams, S. R.; Gadian, D. G., q-Space imaging of the brain. *Magn Reson Med* **1994,** *32* (6), 707-13.
21. Pages, G.; Yau, T. W.; Kuchel, P. W., Erythrocyte Shape Reversion From Echinocytes to Discocytes: Kinetics via Fast-Measurement NMR Diffusion-Diffraction. *Magnetic Resonance in Medicine* **2010,** *64* (3), 645-652.
22. Torres, A. M.; Taurins, A. T.; Regan, D. G.; Chapman, B. E.; Kuchel, P. W., Assignment of coherence features in NMR q-space plots to particular diffusion modes in erythrocyte suspensions. *Journal of Magnetic Resonance* **1999,** *138* (1), 135-143.
23. Cavadini, S.; Dittmer, J.; Antonijevic, S.; Bodenhausen, G., Slow diffusion by singlet state NMR spectroscopy. *J. Am. Chem. Soc.* **2005,** *127*, 15744-15748.
24. Ahuja, P.; Sarkar, R.; Vasos, P. R.; Bodenhausen, G., Diffusion coefficients of biomolecules using long-lived spin states. *Journal of the American Chemical Society* **2009,** *131* (22), 7498-7499.
25. Sarkar, R.; Ahuja, P.; Vasos, P. R.; Bodenhausen, G., Measurement of slow diffusion coefficients of molecules with arbitrary scalar couplings via long-lived spin states. *ChemPhysChem* **2008,** *9* (16), 2414-2419.
26. Sarkar, R.; Vasos, P. R.; Bodenhausen, G., Singlet-State exchange NMR spectroscopy for the study of very slow dynamic processes. *J. Am. Chem. Soc.* **2007,** *129* (2), 328-334.
27. Cavadini, S.; Vasos, P. R., Singlet states open the way to longer time-scales in the measurement of diffusion by NMR spectroscopy. *Concepts in Magnetic Resonance Part A* **2008,** *32A* (1), 68-78.
28. Yadav, N. N.; Torres, A. M.; Price, W. S., NMR q-space imaging of macroscopic pores using singlet spin states. *J Magn Reson* **2010,** *204* (2), 346-8.
29. Torres, A. M.; Ghadirian, B.; Price, W. S., Diffusion-diffraction using singlet spin states and various NMR coherences in a J-coupled AX spin system. *RSC Advances* **2012,** *2* (8), 3352-3360.
30. Tanner, J. E.; Stejskal, E. O., Restricted self diffusion of protons in colloidal systems by pulsed-gradient spin echo methods. *J. Chem. Phys.* **1968,** *49*, 1768.
31. Callaghan, P. T., Pulsed-Gradient Spin-Echo NMR for planar, cylindrical, and spherical pores under conditions of wall relaxation. *J Magn Reson Ser A* **1995,** *113* (1), 53-59.
32. Frey, S.; Kärger, J.; Pfeifer, H.; Walther, P., NMR self-diffusion measurements in regions confined by "absorbing" walls. *Journal of Magnetic Resonance (1969)* **1988,** *79* (2), 336-342.
33. Lennon, A. J.; Kuchel, P. W., Enhancement of the Diffraction-Like Effect in Nmr Diffusion Experiments. *J Magn Reson Ser A* **1994,** *111* (2), 208-211.
34. Pileio, G.; Carravetta, M.; Levitt, M. H., Storage of nuclear magnetization as long-lived singlet order in low magnetic field. *Proceedings of the National Academy of Sciences* **2010,** *107* (40), 17135-17139.

35. Tayler, M. C. D.; Levitt, M. H., Singlet nuclear magnetic resonance of nearly-equivalent spins. *Physical Chemistry Chemical Physics* **2011,** *13* (13), 5556-5560.
36. Tayler, M. C. D.; Levitt, M. H., Accessing long-lived nuclear spin order by isotope-induced symmetry breaking. *Journal of the American Chemical Society* **2013,** *135* (6), 2120-2123.
37. Pileio, G., Singlet NMR methodology in two-spin-1/2 systems. *Prog Nucl Magn Reson Spectrosc* **2017,** *98-99*, 1-19.
38. Bengs, C.; Levitt, M. H., SpinDynamica: Symbolic and numerical magnetic resonance in a Mathematica environment. *Magn Reson Chem* **2017**.
39. Pileio, G.; Dumez, J.-N.; Pop, I.-A.; Hill-Cousins, J. T.; Brown, R. C. D., Real-space imaging of macroscopic diffusion and slow flow by singlet tagging MRI. *Journal of Magnetic Resonance* **2015,** *252* (0), 130-134.
40. Dumez, J. N.; Hill-Cousins, J. T.; Brown, R. C. D.; Pileio, G., Long-lived localization in magnetic resonance imaging. *Journal of Magnetic Resonance* **2014,** *246*, 27-30.
41. Carravetta, M.; Levitt, M. H., Long-lived nuclear spin states in high-field solution NMR. *J. Am. Chem. Soc.* **2004,** *126*, 6228-6229.
42. Pileio, G.; Hill-Cousins, J. T.; Mitchell, S.; Kuprov, I.; Brown, L. J.; Brown, R. C. D.; Levitt, M. H., Long-lived nuclear singlet order in near-equivalent 13C spin pairs. *Journal of the American Chemical Society* **2012,** *134* (42), 17494-17497.
43. Pileio, G.; Carravetta, M.; Hughes, E.; Levitt, M. H., The long-lived nuclear singlet state of 15N-nitrous oxide in solution. *J. Am. Chem. Soc.* **2008,** *130* (38), 12582-12583.
44. Stevanato, G.; Hill-Cousins, J. T.; Håkansson, P.; Roy, S. S.; Brown, L. J.; Brown, R. C. D.; Pileio, G.; Levitt, M. H., A nuclear singlet lifetime of more than one hour in room-temperature solution. *Angewandte Chemie International Edition* **2015,** *54*, 3740–3743.